Kinetics and Slurry-type Reactor Modelling during Catalytic Hydrogenation of *o*-Cresol on Ni/SiO_2

HABIB HICHRI, ARMAND ACCARY and JULIEN ANDRIEU*

Laboratoire d'Automatique et de Génie des Procédés (LAGEP), Université Claude Bernard, Lyon I, U.R.A. C.N.R.S. D1328, Bât. 305, 43 Boulevard du 11 novembre 1918, 69622 Villeurbanne Cédex (France)

(Received April 2, 1991; in final form September 27, 1991)

Abstract

The effect of kinetic parameters (reactant concentrations, temperature) was investigated on the initial reaction rate for the catalytic hydrogenation of *o*-cresol on Ni/SiO_2, carried out in a batch or semi-batch agitated slurry-type reactor.

The data were interpreted by a kinetic model based on the Langmuir–Hinshelwood mechanism with non-dissociative and non-competitive adsorption of *o*-cresol and hydrogen on different sites, where the limiting step is due to the reaction of adsorbed reactants. The activation energy ($E_a = 82$ kJ/mol) is in good agreement with previous literature values reported for the catalytic hydrogenation of phenol.

Taking into account thermodynamic (solubilities) and mass transfer kinetics (k_La) data measured *in situ*, the integral reactor conversion rate of this three-phase catalytic reaction was simulated accurately in the physical regime by taking into account external and internal mass transfer resistances.

Keywords: kinetics, hydrogenation, modelling, reactor, nickel catalyst.

Introduction

Many industrial catalytic reactions such as hydrogenation, Fischer–Tropsch synthesis, oxidation, etc., are carried out in three-phase systems like agitated slurries or continuous bubble columns with suspended catalyst particles. Data concerning the kinetic aspects of these reactions are numerous in the literature [1–7]; in contrast, there are few results concerning integral reactor modelling taking into account mass transfer phenomena, that is, the coupling effects of reaction and diffusion inside the reactive medium [8–13]. The industrial hydrogenation of phenolic compounds and their derivatives currently uses this reactor type (perfumes, painting industry, etc.).

Therefore, we chose to study a simple reaction model, namely, the hydrogenation of *o*-cresol on silica-supported nickel catalyst using isopropanol as a solvent in the temperature range 393–413 K and under hydrogen partial pressures from 1 to 30 bar. Furthermore, for this irreversible simple reaction, there are kinetics data available in the literature [1, 3–6].

The aim of the present work was firstly to determine precisely the intrinsic kinetics of this liquid-phase hydrogenation reaction, and secondly to use these results with thermodynamic and mass transfer data previously obtained [14] to set up an integral laboratory reactor model taking into account kinetic and mass transfer effects.

2. Materials and methods [14]

The reactor (Fig. 1) consists of a stainless steel autoclave equipped with a self gas-inducing agitator mounted on a hollow shaft. All the geometric characteristics of the system are shown in Table 1.

This apparatus was equipped with a temperature regulator (± 1 °C) and convenient safety devices. Hydrogen is introduced through a pressure reducer which controls the gas pressure inside the reactor. The catalyst was a commercial nickel (50% by mass) supported on silica, manufactured by Mallinkrodt (Table 2).

All the experiments were conducted using the same catalyst sample and isopropanol as a solvent with high initial concentrations of *o*-cresol ($b_{L,0} = 2.0$ kmol m^{-3}). The freshly prepared catalyst being pyrophoric, it was necessary to keep it in a safe inactive form by CO_2 adsorption. So, before each run a reactivation protocol was set up and rigorously respected during all the experiments. The *o*-cresol conversion rate was followed either by liquid-phase

*To whom correspondence should be addressed.

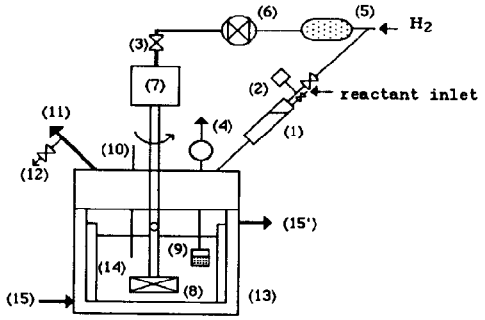

Fig. 1. Experimental set-up: 1, reactant tank; 2, absolute pressure sensor; 3, valve; 4, liquid sample valve; 5, gas filter; 6, manual pressure reducer; 7, electric motor; 8, turbine; 9, sample filter; 10, thermocouple; 11, safety valve; 12, gas outlet; 13, jacket; 14, baffles; 15–15', constant temperature bath.

TABLE 1. Geometric characteristics of the reactor system

Reactor volume, V_r	0.15×10^{-3} m^3
Inside diameter, D_R	4.97×10^{-2} m
Turbine diameter, D	2.92×10^{-2} m
Turbine height from bottom, h_0	1.4×10^{-2} m
Liquid volume, V_L	$0.066-0.1 \times 10^{-3}$ m^3
Baffles: number and width	4 at 90°; $l = 10^{-2}$ m

TABLE 2. Textural characteristics of the catalyst Ni/SiO_2 (manufactured by Mallinkrodt)

Commercial presentation	Spheres, 8 × 14 mesh
Granulometry	$40 < d_p < 400$ μm
Apparent density	$\rho_p = 929$ kg m^{-3}
Specific area	$s_g = 200 \times 10^3$ m^2 kg^{-1}
Pore volume	$v_p = 0.43 \times 10^{-3}$ m^3 kg^{-1}

sampling (1–2 ml) when the reactor operates under constant hydrogen pressure (semi-batch) or by gas-phase pressure acquisition when the reactor operates in batch mode. Liquid samples were analysed by GPC (internal standard method) with a 1% accuracy. The reproducibility of initial rates was around 5%.

3. Results and discussion

3.1. Preliminary runs

3.1.1. Experimental domain

In order to simplify the modelling problem, the first approach was to define experimental conditions (P, T, o-cresol concentration) where the following simple stoichiometry is observed:

$$H_2 + \tfrac{1}{3}o\text{-cresol} \rightarrow \tfrac{1}{3}(2\text{-methylcyclohexanol})$$

Many authors [3–6] have observed, for this hydrogenation catalysed by supported metals (Pt, Pd, etc.), a series-type stoichiometry with formation of an intermediate product, 2-methylcyclohexanone.

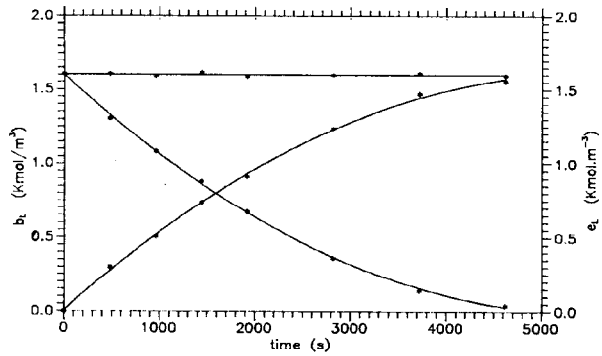

Fig. 2. Reactant and product profile versus time. ($T = 413$ K, $P_{H_2} = 1.5$ MPa, $m_c = 55.64$ kg/m^3 disp., $N = 1200$ rpm, $V_L = 69.3 \times 10^{-6}$ m^3, $d_p = 71.5$ μm.)

Therefore, we have tried to characterize this formation by chromatographic analysis and by the mass balance equation; under our conditions we did not observe any significant amount of this intermediate ketonic compound (see Fig. 2).

3.1.2. Solubilities and gas–liquid mass transfer data

The hydrogen solubility and volumetric gas–liquid mass transfer coefficients, k_La, were previously measured *in situ* in an organic medium using the hydrogen absorption kinetics method. The solubility data were measured for the pure compounds, namely, o-cresol and isopropanol, and also for a binary mixture of these compounds. Some of these results are shown in Table 3. Furthermore, the hydrogen solubility results concerning the o-cresol + isopropanol mixture were interpreted by the following relationship [14, 15]:

$$\ln He_{mix} = \sum_i X_i \ln He_i - (1.959 - 594.273/T)X_1X_2 \quad (1)$$

where X_i represents the mole fraction of component i in the mixture and T the absolute temperature.

The k_La values obtained for various experimental conditions (agitation speed, temperature, fluid prop-

TABLE 3. Solubility results as a function of temperature

Liquid	T (K)	10^8 He (Pa m^3 kmol^{-1})
Isopropanol	308	0.292
	318	0.290
	333	0.273
	343	0.267
o-Cresol	313	0.794
	353	0.608
	393	0.523
Molar mixture	313	0.400
(30% o-cresol +	323	0.376
70% isopropanol)	333	0.362
	343	0.348

erties, etc.) were correlated by the following dimensionless relation [14]:

$$Sh = 5 \times 10^{-3} Re^{0.717} Sc^{0.5} We^{1.17} \quad (2)$$

3.1.3. Experimental conditions of the chemical regime

In order to identify the intrinsic kinetic parameters we checked, under the more critical experimental conditions of high temperature, high concentration and high catalyst loading, that the mass transfer effects were eliminated. Indeed, Fig. 3 shows that the reaction rate R_A increases up to 800 rpm then reaches an asymptotic value beyond which the external mass transfer effects are negligible. Adopting the experimental conditions at this plateau, we confirmed the kinetic regime of the reaction by running different experiments with different catalyst loads denoted by m_c. The experimental results were plotted classically using

$$\frac{1}{R_A} = f\left(\frac{1}{m_c}\right)$$

This plot is quasi-linear and passes through the origin (see Fig. 4). It confirms that for the given agitation conditions ($N > 800$ rpm) the external gas–liquid mass transfer resistance is negligible. The absence of external liquid–solid and internal mass transfer resistance was checked previously by evaluating the criteria proposed in refs. 8 and 9. For example, the generalized Thiele modulus value was less than 1 ($\Phi'_s \leqslant 1$). Furthermore, this estimate was confirmed experimentally by runs with different particle catalyst sizes [14].

3.2. Kinetic model of the reaction

Firstly, experimental results, presented elsewhere [14], show that the reaction product, 2-methylcyclohexanol, has no kinetic effect on the reaction rate under our experimental conditions. Subsequently, numerous runs were carried out to study the influence of the dissolved hydrogen concentration for constant initial *o*-cresol concentration at three temperatures. In order to eliminate the possible inhibiting effects of the reaction products, the initial reaction rate, $r_{m,0}$, was obtained by numerical differentiation of the curves $b_L(t)$ at time zero ($t = 0$). The initial reaction rates $r_{m,0}$ plotted in Fig. 5 show a fractional reaction order continuously decreasing with the hydrogen concentration. This curve type is often observed in heterogeneous catalysis when the

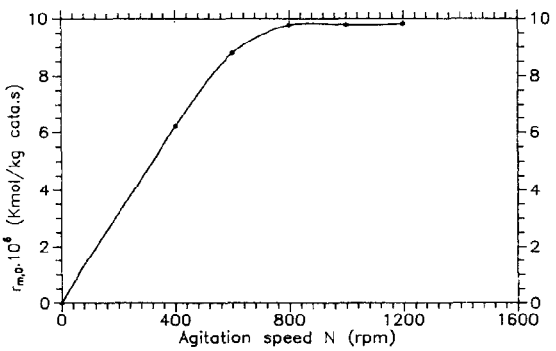

Fig. 3. Evolution of initial revolution rate with agitation speed. ($T = 413$ K, $P_{H_2} = 1.5$ MPa, $m_c = 55.64$ kg/m^3 disp., $b_{L,0} = 2.0$ kmol/m^3, $V_L = 69.3 \times 10^{-6}$ m^3, $d_p = 56.5$ μm.)

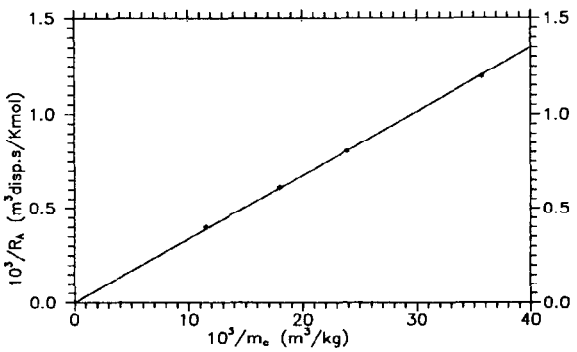

Fig. 4. Influence of catalyst loading on the initial reaction rate. ($T = 413$ K, $P_{H_2} = 1.5$ MPa, $d_p = 71.5$ μm, $N = 1200$ rpm, $b_{L,0} = 2.0$ kmol/m.)

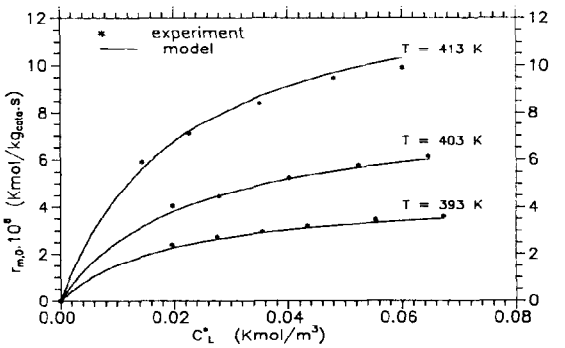

Fig. 5. Influence of dissolved hydrogen concentration on the initial activity of the catalyst. ($m_c = 55.64$ kg/m^3 disp., $V_L = 69.3 \times 10^{-6}$ m^3, $b_{L,0} = 2.0$ kmol/m^3, $d_p = 71.5$ μm, $N = 1200$ rpm.)

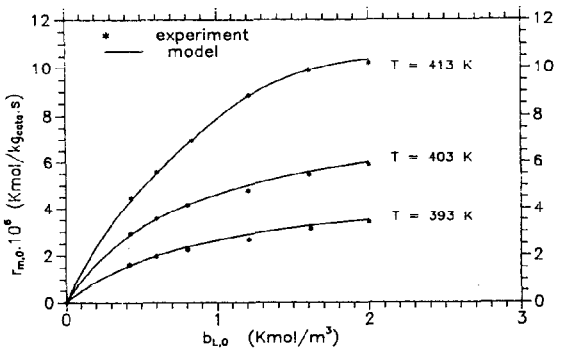

Fig. 6. Influence of *o*-cresol concentration on the initial activity of the catalyst. ($m_c = 55.64$ kg/m^3 disp., $V_L = 69.3 \times 10^{-6}$ m, $P_t = 2.0$ MPa, $d_p = 71.5$ μm, $N = 1200$ rpm.)

available sites are progressively occupied. Furthermore, Fig. 6 shows the influence of the *o*-cresol concentration at constant hydrogen partial pressures for the same three temperatures. The plots are similar to those presented in Fig. 5, thus the same qualitative conclusions can be inferred. From the literature, amongst the various possible elementary phenomena occurring in series (adsorption, reaction, desorption) which govern the overall microkinetics rate, the most probable limiting step seems to be the reaction step in the adsorbed state [11, 16]. Following these observations, we have tried to identify one of the kinetic models shown in Table 4. It is well known that these models differ according to the hydrogen adsorption mode, either dissociated (D), or not dissociated (ND), and by the number of sites involved [17].

Identification of the model parameters was realized by using the Marquardt algorithm [18] with least square minimization between the experimental and calculated values for each temperature. As indicated by Table 5, model 6 leads to the lowest mean relative error (3%) with a coherent variation of the kinetic parameters (K_A, K_B and k) as a function of the temperature. Nevertheless, it can be seen that models 1 and 7, where hydrogen can be adsorbed on the same sites as *o*-cresol, lead to very similar mean square relative errors. Owing to our severe reaction

TABLE 4. Mechanism and the corresponding kinetic models

Model no.	No. of sites	Hydrogen adsorption	Substrate adsorption	Reaction rate r_m
1	2	AND	BC	$k\frac{K_A K_B c_L b_L}{(1+K_A c_L+K_B b_L)^2}$
2	3	AD	BC	$k\frac{K_A K_B c_L b_L}{[1+(K_A c_L)^{1/2}+K_B b_L]^3}$
3	1	AND	BN	$k\frac{K_A c_L b_L}{1+K_A c_L}$
4	3	AD	BNC	$k\frac{K_A K_B c_L b_L}{[1+(K_A c_L)^{1/2}]^2(1+K_B b_L)}$
5	2	AD	BN	$k\frac{K_A c_L b_L}{[1+(K_A c_L)^{1/2}]^2}$
6	2	AND	BNC	$k\frac{K_A K_B c_L b_L}{(1+K_A c_L)(1+K_B b_L)}$
7	2	AND	BNC	$k\frac{K_A K_B c_L b_L}{(1+K_A c_L+K_B b_L)(1+K_B b_L)}$

AD = dissociative adsorption; AND = non-dissociative adsorption; BC = competitive adsorption; BNC = non-competitive adsorption; BN = not adsorbed.

TABLE 5. Error estimations for the different kinetic models

Model no.	T (K)	$k \times 10^5$ (kmol/kg cat s)	K_A (m^3/kmol)	K_B (m^3/kmol)	Average relative error (%)	Residual sum (kmol/kg cat s)
1	393	1.58 ± 0.14	96.3 ± 40	2.71 ± 1.64	3	8.03×10^{-8}
	403	2.75 ± 0.20	87.1 ± 26.4	2.58 ± 0.79	2.3	1.16×10^{-7}
	413	5.7 ± 0.55	49.1 ± 10.8	1.19 ± 0.28	2.67	2.03×10^{-8}
2	393	5.53 ± 1.17	57.2 ± 26.6	0.562 ± 0.147	5	1.16×10^{-7}
	403	5.86 ± 3.86	211 ± 514	1.2 ± 1.5	6	2.61×10^{-7}
	413	8.76 ± 6.28	335 ± 980	1.29 ± 2.02	8	5.68×10^{-7}
3	393	0.318 ± 0.082	29.6 ± 15.5		16.5	3.26×10^{-7}
	403	0.59 ± 0.18	25.7 ± 15.1		17.45	6.22×10^{-7}
	413	0.996 ± 0.974	27.7 ± 14.4		15.74	1.01×10^{-6}
4	393	7.77 ± 22.20	2.82 ± 8.78	0.46 ± 0.88	17.0	3.90×10^{-7}
	403	8.85 ± 15.7	3.05 ± 6.22	0.69 ± 0.84	18.3	7.55×10^{-7}
	413	28.4 ± 103.2	3.42 ± 12.78	0.358 ± 0.91	16.6	1.26×10^{-6}
5	393	0.729 ± 0.388	21.1 ± 21.2		17.5	3.53×10^{-7}
	403	1.47 ± 0.98	16.0 ± 18.9		19.0	6.94×10^{-7}
	413	2.43 ± 1.43	18.0 ± 18.8		17.0	1.12×10^{-6}
6	393	0.677 ± 0.047	49.8 ± 4.74	1.02 ± 0.11	2.98	7.60×10^{-8}
	403	1.15 ± 0.05	44.9 ± 2.9	1.17 ± 0.08	1.95	8.56×10^{-8}
	413	2.29 ± 0.18	46.3 ± 4.38	0.798 ± 0.085	2.8	2.09×10^{-7}
7	393	0.749 ± 0.071	127 ± 18	0.752 ± 0.998	3.4	8.49×10^{-8}
	403	1.27 ± 0.09	123.0 ± 13.5	0.834 ± 0.081	2.3	1.02×10^{-7}
	413	2.57 ± 0.20	103.0 ± 10.4	0.59 ± 0.06	2.4	1.76×10^{-7}

conditions, particularly for pressure, it was not possible to characterize the adsorbed species type by spectrometric techniques in order to establish supplementary experimental confirmation for model 6 (Table 5).

This kinetic model discrimination does not influence the integral reactor modelling because the two models lead to kinetic rate equations with very similar adjustment precision. So, we have adopted a mechanism where the hydrogen and *o*-cresol are adsorbed on different sites, without dissociation of hydrogen, and where the reaction between adsorbed species is the limiting step. This mechanism leads to the following kinetic rate equation:

$$r_m = k \frac{K_A K_B c_L b_L}{(1 + K_A c_L)(1 + K_B b_L)} \tag{3}$$

where

$$k\,(\text{kmol/kg s}) = 5.46 \times 10^5 \exp(-82220/RT) \tag{4}$$

$$K_A\,(\text{m}^3/\text{kmol}) = 1.055 \times 10 \exp(+5003/RT) \tag{5}$$

$$K_B\,(\text{m}^3/\text{kmol}) = 7.54 \times 10^{-3} \exp(+16325/RT) \tag{6}$$

The activation energy, $E_a = 82.2$ kJ/mol, is very close to the value obtained by Bühlmann [6] for the same hydrogenation reaction with Ni catalyst (82.8 kJ/mol). This high value, which is in good agreement with most of the results in the literature concerning catalytic hydrogenation, confirms experimentally the absence of intraparticle diffusion effects for our experimental conditions.

3.3. *Laboratory reactor modelling*

3.3.1. *Theory*

From the microkinetics and macrokinetics data, it was possible to simulate integral conversion runs of the laboratory reactor operating in the physical or chemical regime in batch or semi-batch (p_{H_2} = constant) conditions. Supposing that the dissolved hydrogen is the limiting reactant, with no resistance in the gas film, and that the reactor is isothermal and perfectly mixed, the hydrogen solubility c_L^* given by Henry's law is uniform (batch) or constant and uniform (semi-batch). Thus, we can deduce the following equations for the model.

For the *gas phase*, the hydrogen mass balance is

$$-\frac{V_g}{RT}\frac{dp}{dt} = k_L a V_L (c_L^* - c_L) \tag{7}$$

This equation does not appear when the reactor is in the semi-batch mode (c_L^* = constant).

For the *liquid phase*, concerning hydrogen,

$$k_L a(c_L^* - c_L) = k_s a_p (c_L - c_s) + \frac{dc_L}{dt} \tag{8}$$

$$k_s a_p (c_L - c_s) = r_m(c_s, b_s) m_c \eta_c = R_A \tag{9}$$

The catalyst effectiveness, η_c, is calculated assuming spherical particles and using the generalized Thiele modulus, Φ_L, as defined by Bischoff [19]:

$$\Phi_L = \frac{R_0}{3}\rho_p r_m(c_s, b_s)\left[\int_0^{c_s} 2\,D_{e,A}\rho_p r_m(c, b_s)dc\right]^{-1/2} \tag{10}$$

with

$$\eta_c = \frac{1}{\Phi_L}\left[\coth(3\Phi_L) - \frac{1}{3\Phi_L}\right] \tag{11}$$

Concerning *o*-cresol and *o*-methylcyclohexanol

$$\frac{de_L}{dt} = -\frac{db_L}{dt} = k_s' a_p (b_L - b_s)$$
$$= \nu_B R_A$$
$$= \nu_B k_s a_p (c_L - c_s) = R_B \tag{12}$$

The initial conditions are

$$t = 0, \quad p_{H_2,0} = \text{He}_{mix} c_{L,0}^*; \quad b_L = b_{L,0}$$

The hydrogen solubility is calculated at each time by taking into account the pressure variations (batch mode) and the changes in the liquid-phase composition. The volumetric gas–liquid mass transfer coefficient is calculated from our previous correlation [14] and assumed to be constant during each experiment at T and N constant.

The liquid–solid mass transfer coefficient values for hydrogen and *o*-cresol, denoted respectively by k_s and k_s' were calculated from literature correlations [8, 9, 14].

3.3.2. *Experimental data interpretation*

All the experiments were carried out in semi-batch or batch isothermal conditions, with respect to hydrogen, over a wide range of reactant concentrations and operating conditions in order to check the coherence and the validity of the mass transfer and kinetic parameters previously obtained.

(*a*) *Semi-batch experiments*

Influence of temperature. Many integral reactor runs were carried out at three different temperatures and for various agitation speeds.

For example, the experimental data corresponding to temperatures of 393 and 413 K are presented in Fig. 7 for particles of diameter $d_p = 130$ μm. These

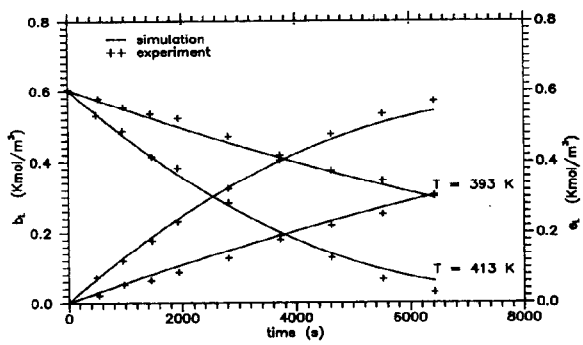

Fig. 7. Concentration profile of *o*-cresol and 2-methylcyclohexanol as a function of time for semi-batch runs. ($b_{L,0} = 0.6$ kmol/m^3, $P_t = 0.9$ MPa, $m_c = 53$ kg/m^3 disp., $N = 1200$ rpm, $V_L = 69.3 \times 10^{-6}$ m^3, $d_p = 100$–160 μm.)

plots show that the experimental results are predicted well by the model and that the temperature has a strong influence on the conversion rate (kinetic regime).

Influence of the agitation speed. External mass transfer rates at the gas–liquid interface ($k_L a$) and at the liquid–solid interface ($k_s a_p$) are mainly dependent on the agitation speed. As shown in Figs. 8 and 9, this effect is more apparent when the agitation speed is low, that is, when the reactor is under physical regime control, as predicted by the reactor model. At high agitation frequencies ($N > 800$ rpm) the conversion rate becomes independent of the agitation conditions (Fig. 10); this variation is again predicted well by the model. Under these agitation conditions, the external mass transfer gradients at the gas–liquid interface, $\Delta c_L/c_L^*$, or at the liquid–solid interface, $\Delta c_s/c_s$, are very low, but these resistances increase at low agitation speeds when the gas–liquid resistance becomes predominant (Fig. 11). With regard to internal mass transfer resistances, Fig. 12 shows, in the case of the largest particles, some typical calculated values of the Thiele modulus and effectiveness factors.

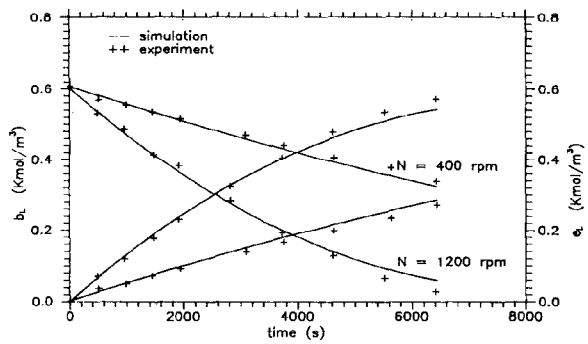

Fig. 8. Concentration profile of *o*-cresol and 2-methylcyclohexanol as a function of time for semi-batch runs. ($T = 413$ K, $P_t = 0.9$ MPa, $m_c = 53$ kg/m^3 disp., $b_{L,0} = 0.6$ kmol/m^3, $V_L = 69.3 \times 10^{-6}$ m^3, $d_p = 100$–160 μm.)

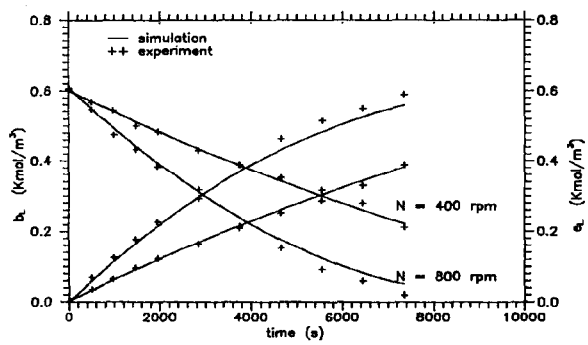

Fig. 9. Concentration profile of *o*-cresol and 2-methylcyclohexanol as a function of time for semi-batch runs. ($T = 413$ K, $P_t = 0.9$ MPa, $m_c = 55.5$ kg/m^3 disp., $b_{L,0} = 0.6$ kmol/m^3, $V_L = 69.4 \times 10^{-6}$ m^3, $d_p = 225$ μm.)

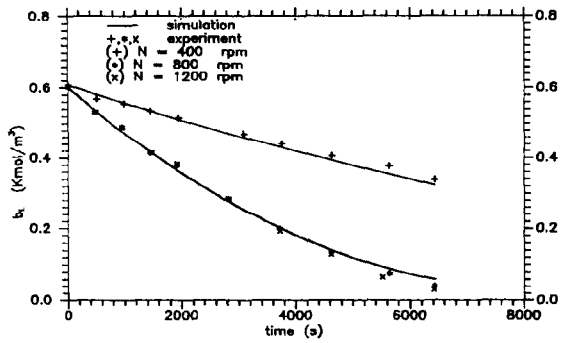

Fig. 10. Influence of agitation speed on the evolution of the *o*-cresol profile for semi-batch runs. ($T = 413$ K, $P_t = 0.9$ MPa, $m_c = 53$ kg/m^3 disp., $b_{L,0} = 0.6$ kmol/m^3, $V_L = 69.3 \times 10^{-6}$ m^3, $d_p = 100$–160 μm.)

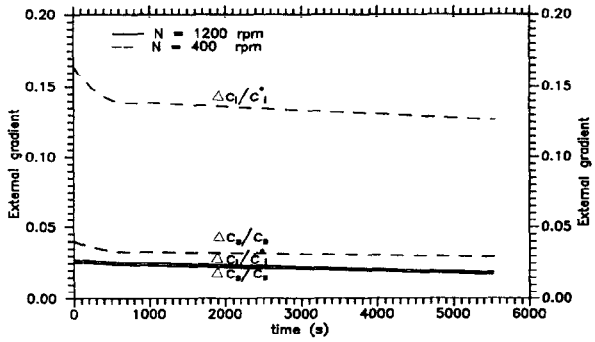

Fig. 11. Estimation of external gas liquid and liquid–solid mass-transfer gradients (semi-batch runs). ($b_{L,0} = 0.6$ kmol/m^3, $P_t = 0.9$ MPa, $m_c = 53$ kg/m^3 disp., $T = 393$ K, $V_L = 69.3 \times 10^{-6}$ m^3, $d_p = 100$–160 μm.)

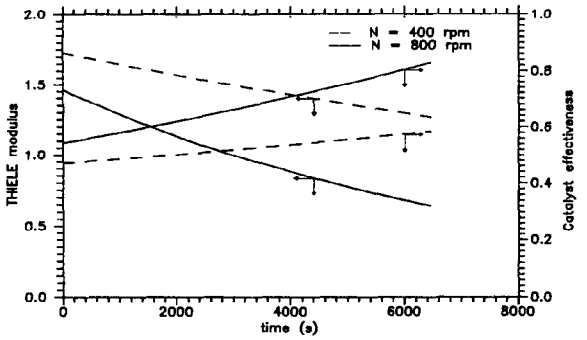

Fig. 12. Catalyst effectiveness and Thiele modulus as a function of time for semi-batch runs. ($T = 413$ K, $P_t = 0.9$ MPa, $b_{L,0} = 0.6$ kmol/m^3, $m_c = 55.64$ kg/m^3 disp., $V_L = 69.3 \times 10^{-6}$ m, $d_p = 225$ μm.)

(*b*) *Batch experiments*

The conditions correspond to those occurring frequently in the laboratory autoclaves. In this case, *o*-cresol and dissolved hydrogen concentrations continuously decrease as a function of time, so that the total pressure recording offers an easy method to

follow the conversion rate. Therefore, different experiments were conducted by varying the catalyst loading, temperature and agitation speed separately.

Influence of catalyst loading. Figure 13 shows that the model is able to represent the total pressure evolution accurately inside the reactor as a function of time and that the conversion rate is an increasing function of the catalyst loading.

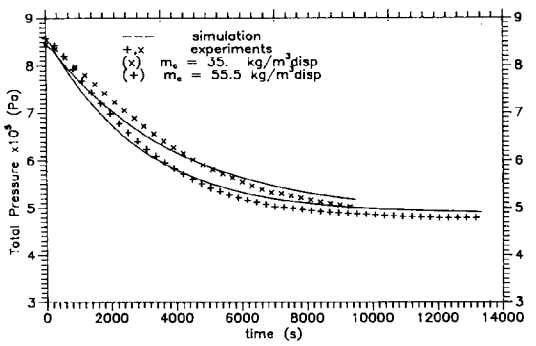

Fig. 13. Total pressure variation inside the reactor as a function of time for batch runs. ($N = 400$ rpm, $T = 403$ K, $P_{H_2} = 0.375$ MPa, $b_{L,0} = 0.6$ kmol/m^3, $V_L = 69.6 \times 10^{-6}$ m, $d_p =$ 250 315 μm.)

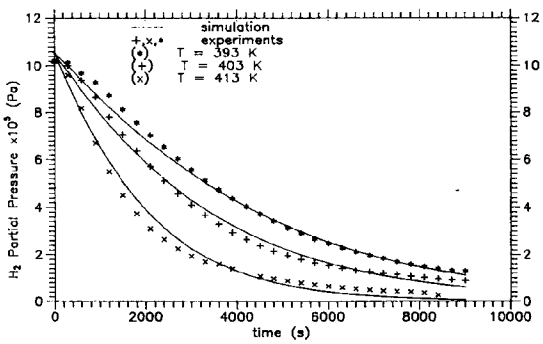

Fig. 14. Evolution of hydrogen partial pressure for different temperatures for batch runs. ($N = 1200$ rpm, $m_c = 35$ kg/m^3 disp., $V_g = 104 \times 10^{-6}$ m^3, $b_{L,0} = 0.6$ kmol/m^3, $V_L = 69.6 \times 10^{-6}$ m^3, $d_p = 160$–200 μm.)

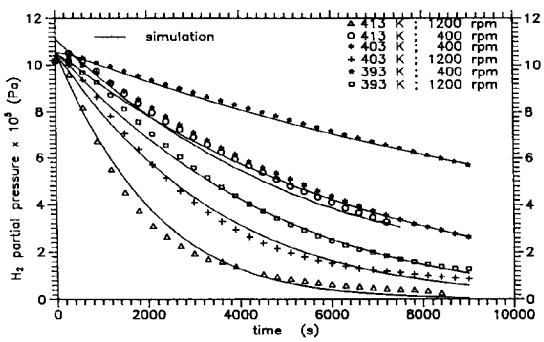

Fig. 15. Evolution of hydrogen partial pressure inside the reactor as a function of time: influence of the agitation speed for batch runs. ($b_{L,0} = 0.6$ kmol/m^3, $m_c = 35$ kg/m^3 disp., $V_g = 104 \times 10^{-6}$ m^3, $d_p = 160$–200 μm, $V_L = 69.6 \times 10^{-6}$ m^3.)

Influence of temperature. Figure 14 shows that the hydrogen concentration profile is very sensitive to the temperature variation and that this influence is more important when the kinetic regime is reached. This variation is again predicted well by the reactor simulation and is mainly related to the high value of the hydrogenation activation energy.

Influence of the agitation speed. Figure 15 shows that the effect of agitation speed on the conversion rate is similar to that observed in the case of semi-batch experiments; thus we confirm that this parameter becomes predominant in the physical regime, that is, at low agitation speeds.

4. Conclusions

Between 393 and 413 K, the catalytic hydrogenation intrinsic kinetics of *o*-cresol on Ni/SiO_2 using isopropanol as solvent were interpeted by a Langmuir–Hinshelwood model with non-competitive and non-dissociative adsorption of hydrogen and *o*-cresol on different sites. The activation energy was around 82 kJ/mol, which is in good agreement with the literature values for catalytic hydrogenation.

These data, used jointly with thermodynamic (solubilities) and hydrodynamic ($k_L a$) data measured *in situ* on the organic medium, allowed us to simulate the reactor yield in the chemical and physical regimes when internal and external hydrogen mass transfer resistances appear.

For this simple catalytic reaction, this modelling approach can be used for design and scale-up of industrial reactors from laboratory data as soon as the hydrodynamic characteristics of the reactor in an organic medium are available (principally, $k_L a$ values).

Acknowledgements

The authors are grateful to Society Rhône–Poulenc and Mallinkrodt for the material support received during this work.

Nomenclature

a	gas–liquid interfacial area, m^2 m^{-3}
a_p	liquid–solid interfacial area, m^2 m^{-3}
b_L	*o*-cresol concentration, kmol m^{-3}
c_L	dissolved hydrogen concentration, kmol m^{-3}
c_L^*	equilibrium concentration of dissolved hydrogen, kmol m^{-3}
D_R, D	reactor and turbine diameter, respectively, m
D_A, $D_{e,A}$	molecular and effective diffusivity of H_2, m^2 s^{-1}
d_p	catalyst bead diameter, m
E_a	activation energy, kJ mol^{-1}
e	methylcyclohexanol concentration, kmol m^{-3}

He	Henry's constant, Pa m^3 $kmol^{-1}$
K_A, K_B	adsorption constants, m^3 $kmol^{-1}$
k	reaction rate, kmol kg^{-1} s^{-1}
k_L, k_s	hydrogen gas–liquid and liquid–solid mass transfer coefficients, m s^{-1}
k'_s	*o*-cresol liquid–solid mass transfer coefficient, m s^{-1}
N', N	agitation speed, Hz or rpm
m_c	catalyst load, kg m^{-3}
P_t	total pressure, Pa
p	hydrogen pressure, Pa
R	gas constant, J mol^{-1} K^{-1}
R_A, R_B	reaction rate, kmol (m^{-3} disp.) s^{-1}
Re	$= \rho_f N' D^2/\mu_f$, Reynolds number
R_0	catalyst bead radius, m
r_m	catalyst initial activity for A or b, kmol (kg cat.)$^{-1}$ s^{-1}
Sc	$= \mu_f/D_A\rho_f$, Schmidt number
Sh	$= k_L a D^2/D_A$, Sherwood number
s_g	catalyst specific area, m^2 kg^{-1}
T	temperature, K
t	time, s
V_g	gas volume, m^3
V_L	liquid volume, m^3
V_r	reactor volume, m^3
v_p	catalyst pore volume, m^3 kg^{-1}
We	$= \rho_f N'^2 D^3/\sigma$, Weber number
X	molar fraction in liquid phase
η_c	catalyst efficiency
Φ_L	generalized Thiele modulus, eqn. (10)
Φ'_s	generalized Thiele modulus for sphere
ρ_f	fluid density, kg m^{-3}
ρ_p	apparent catalyst density, kg m^{-3}
σ	liquid interfacial tension, N m^{-1}
ν	stoichiometric coefficients
μ	fluid dynamic viscosity, Pa s

Indices

A	H_2
B	*o*-cresol
f	fluid
g	gas
L	liquid
s	catalyst area
0	initial time
*	thermodynamic equilibrium

References

1 J. C. Jungers, *et al.*, *Cinétique Chimique Appliquée*, Technip, Paris, 1969, pp. 214–249.
2 F. Coussemant and J. C. Jungers, La cinétique de l'hydrogénation catalytique des phénols, *Bull. Soc. Chim. Belge*, *59* (1950) 295.
3 J. J. Zwicky and G. Gut, Kinetics, poisoning and mass transfer effects in liquid phase hydrogenation of phenolic compounds over a palladium catalyst, *Chem. Eng. Sci.*, *33* (1978) 1363.
4 T. Bühlmann, G. Gut and O. M. Kut, Einfluss der Absorption Geschwindigkeit des Wasserstoffes auf die Global, *Chemia*, *36* (1982) 469.
5 J. J. Zwicky, *Thesis*, ETH, Zurich, Switzerland, no. 6035.
6 T. Bühlmann, *Thesis*, ETH, Zurich, Switzerland, 1983, no. 7115.
7 F. Turek, R. Geike and R. Lange, Liquid-phase hydrogenation of nitrobenzene in a slurry reactor, *Chem. Eng. Process.*, *20* (1986) 213.
8 R. V. Chaudhari and P. A. Ramachandran, Three phase slurry reactors, *AIChE J.*, *26* (1980) 177.
9 P. A. Ramachandran and R. V. Chaudhari, *Three Phase Catalytic Reactor*, Gordon and Breach, New York, 1983.
10 G. Gut, J. Kosinka, A. Prabucki and A. Schuerch, Kinetics of the liquid phase hydrogenation and isomerisation of sunflower seed oil with nickel catalyst, *Chem. Eng. Sci.*, *34* (1979) 1051.
11 R. V. Chaudhari, M. G. Parande, P. A. Ramachandran, P. H. Brahme, H. G. Vadgaonkar and R. Jaganathan, Hydrogenation of butynediol to cis-butenediol catalyzed by Pd-, Zn-, $CaCO_3$. Reactor kinetics and modelling of a batch slurry reactor, *AIChE J.*, *31* (1985) 1891.
12 G. Gut, U. Kut, F. Yuecelen and D. Wagner, Liquid phase hydrogenation: the role of mass and heat transfer in slurry reactors, in L. Cerveny (ed.), *Catalytic Hydrogenation*. Elsevier, Amsterdam, 1986, Ch. 15, pp. 517–545.
13 P. H. Brahme and L. K. Doraiswamy, Modelling of a slurry reaction. Hydrogenation of glucose on RANEY nickel, *Ind. Eng. Chem., Process Des. Dev.*, *15* (1976) 130.
14 H. Hichri, Modélisation de l'hydrogénation catalytique de l'*o*-crésol sur Ni/SiO_2 en réacteur triphasique de type suspension agitée, *Thèse de Doctorat*, Univ. Claude Bernard, Lyon I, France, 1991.
15 R. V. Chaudhari, R. V. Cholap, G. Emig and H. Hofmann, Gas–liquid mass transfer in 'dead-end' autoclave reactors, *Can. J. Chem. Eng.*, *65* (1987) 744.
16 A. K. Gupta, K. K. Bhattacharyya and S. K. Saraf, Kinetics of liquid phase hydrogenation of isooctenes over a supported palladium catalyst, *Indian J. Technol.*, *23* (1985) 184.
17 O. A. Hougen and K. M. Watson, *Chemical Process Principles*, Part III, Wiley, New York 1947.
18 D. W. Marquardt, An algorithm for least-squares estimation of nonlinear parameters, *J. Soc. Ind. Appl. Math.*, *11* (1963) 431.
19 K. B. Bischoff, Effectiveness factors for general reaction rate forms, *AIChE J.*, *11* (1965) 21, 315.